Supporting Information

Economical Pt–Free Catalysts for Counter Electrodes of Dye–Sensitized Solar Cells

Mingxing Wu, Xiao Lin, Yudi Wang, Liang Wang, Wei Guo, Daidi Qi, Xiaojun Peng, Anders Hagfeldt, Michael Grätzel, and Tingli Ma

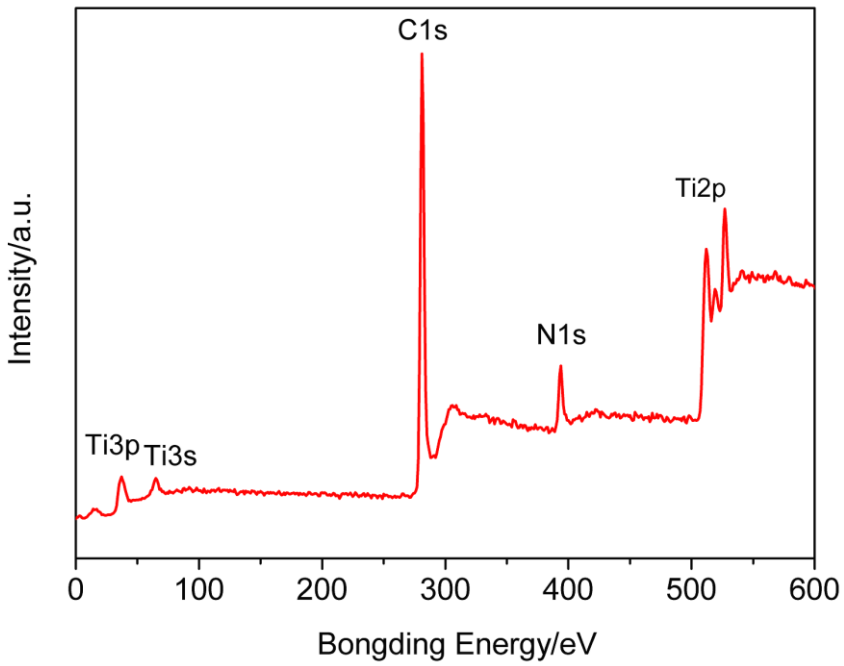

Figure S1. XPS spectra of the as-prepared N doped TiC.

Table S1. Conditions and products, sizes and morphologies of these products. Lattice, TI: Tetragonal Body–centered; TP: Tetragonal Primitive; CF: Cubic Face–centered; HR: Hexagonal R–centered; OP: Orthorhombic Primitive

Metal chloride	Urea/metal chloride molar ratio (R)	Product	Sinter temperature (ºC) and time (h)	Morphology	Lattice	Diameter (nm) by XRD	Diameter (nm) by SEM
	0	TiO_2	800, 3	particle	TI/TP		
$TiCl_4$	5	TiN	800, 3	particle	CF	12.0	10–15
	9	TiC (N)	1100, 3	cube	CF	23.6	15–50
	0	V_2O_3	800, 3	particle	HR	30.7	20–50
$VOCl_3$	5	VN	800, 3	cube	CF	15.4	10–50
	12	VC (N)	1100, 3	cube	CF	44.8	30–150
	0	Cr_2O_3	800, 3	ellipse	HR	54.7	30–80
	1	Cr_2O_3/CrN	800, 3		HR/CF		
	3	CrN/$CrCl_2$	800, 3		CF		
	5	CrN	800, 3	particle		15.5	10–60
$CrCl_3$	7	CrN	800, 3				
	9	CrN	800, 3				
	12	CrN	800, 3				
	12	Cr_3C_2/CrN	1100, 3				
	12	Cr_3C_2	1100, 5	irregular shape	OP	54.5	

We attempted to synthesize zirconium carbide, nitride and oxide using the urea–metal method. However, the attempts to increase the urea ratio and raise the sintering temperature were not effective, and thus we obtained merely ZrO_2 instead of the expected products, ZrC and ZrN. As Figure S2 shown, in the case of R0, ZrO_2 (tetragonal and monoclinic phase) was obtained. As the urea/metal ratio reached 9, a pure tetragonal ZrO_2 was obtained instead of the expected ZrN. The diffraction peaks at 30.16, 35.04, 50.48, 60.02, 74.42, 82.26, and 84.88° can be assigned to the crystal planes of [101], [110], [200], [211], [220], [301] and [222], respectively, for tetragonal ZrO_2 (no. 50–1089, PDF-2 Database). Even when the sintering temperature was increased to 1100 °C, a monoclinic ZrO_2 was obtained instead of the expected ZrC. The diffraction peaks at 24.02, 24.42, 28.16, 31.40, 34.08, 35.24, 38.62, 40.72, 44.80, 45.50, 49.24, 50.14, 50.56, 51.18, 54.02, 55.36, 55.56, 57.12, 58.28, 59.98, 61.32, 61.96, 62.88, 64.24, 65.70, 69.02, 71.12, 72.36, 75.08, 77.50, and 78.90°, can be assigned to the crystal planes of [110], [011],

[$\bar{1}$11], [111], [200], [002], [120], [112], [$\bar{2}$11], [$\bar{2}$02], [220], [022], [$\bar{2}$21], [$\bar{1}$22], [003], [310], [$\bar{3}$11], [113], [$\bar{2}$22], [131], [311], [$\bar{3}$12], [113], [230], [023], [321], [223], [040], [140], [330], and [033], respectively, for monoclinic ZrO_2 (no.37–1484, PDF-2 Database).

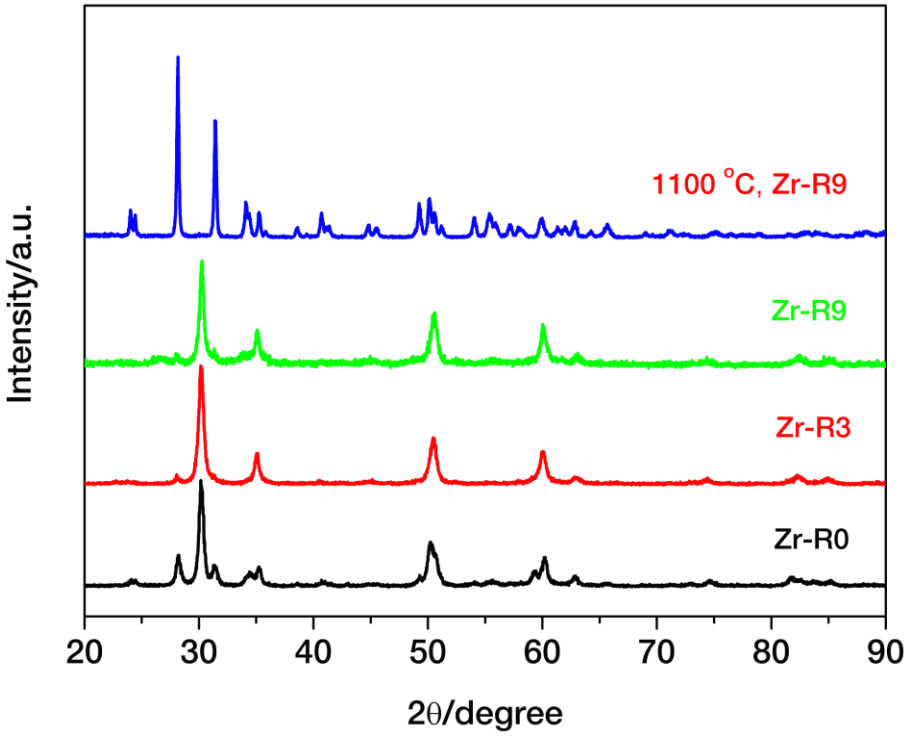

Figure S2. XRD pattern of the as–synthesized ZrO_2. Zr–R0: ZrO_2 (tetragonal and monoclinic phase); Zr–R3 and R9: ZrO_2 (tetragonal phase); Zr–R9, 1100 °C, ZrO_2 (monoclinic phase).

As for niobium, Nb_2O_5, NbN, and NbC (N) were synthesized at the urea/metal chloride ratio of 1, 5 and 12, respectively. As shown in Figure S3, In the black line, the diffraction peaks at 32.78, 34.48, 36.54, 42.54, 45.02, 46.14, 50.44, 50.76, 55.06, 55.28, 58.50, 63.62, and 71.08° can be assigned to the crystal planes of [250], [260], [181], [2100], [330], [002], [321], [380], [182], [202], [2160], [1181], and [382], respectively, for Nb_2O_5 (no. 27–1003, PDF-2, Database). As for the blue line, the diffraction peaks at 36.22, 42.16, 61.20, 72.84, 76.38° can be assigned the crystal planes of [111], [200], [220], [311] and [222], respectively, for NbN (no. 38–1155, PDF-2 Database).

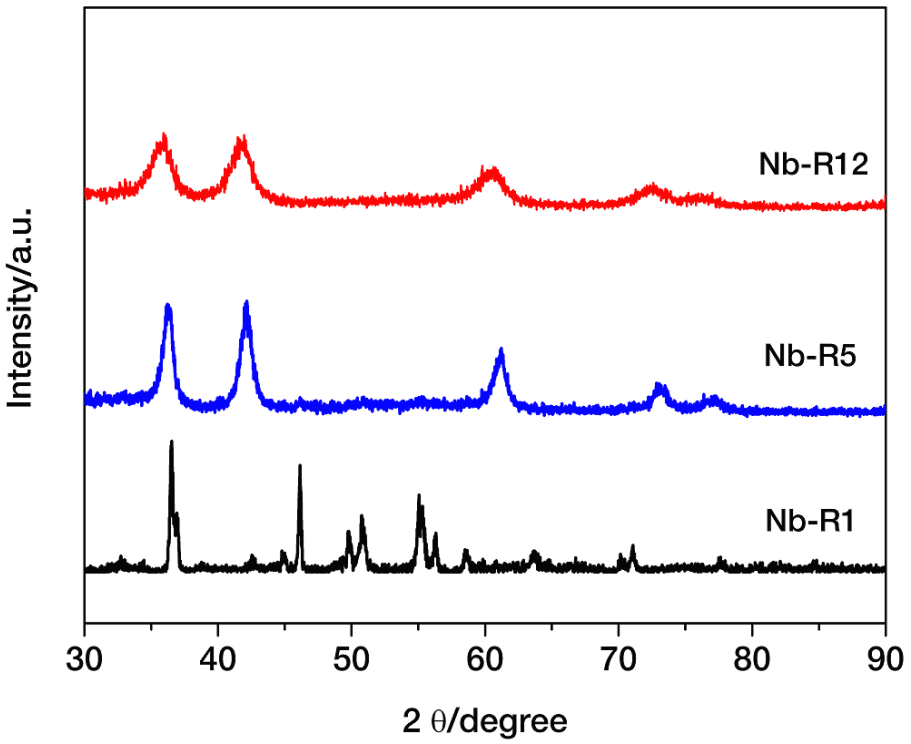

Figure S3. XRD patterns of the as–synthesized Nb_2O_5 (Nb–R1), NbN (Nb–R5), and N doped NbC (Nb–R12).

Unlike the other metal nitrides or carbides, Mo_2N and Mo_2C were synthesized at relative low ratios of urea/metal chloride (R1 and R7). And Mo_2C was obtained at a relative low sintering temperature (800 ºC). As shown in Figure S4, in the case of R0, the diffraction peaks at 26.00, 37.02, 41.64, 49.54, 53.56, 60.20, 63.82, 66.62, 73.22, and 78.78º can be assigned to the crystal planes of [111], [211], [021], [301], [220], [031], [321], [402], [413], and [132], respectively, for MoO_2 (no. 32–0671, PDF-2 Database). As for R1, the diffraction peaks at 37.54, 43.62, 63.36, 76.10, and 80.08 º can be assigned to the planes of [111], [200], [220], [311], and [222], respectively, for γ–Mo_2N (no. 25–1366, PDF-2 Database). For R7, the diffraction peaks at 34.42, 37.64, 39.48, 52.06, 61.94, 69.34, 74.86, 75.76, and 81.28º can be assigned to the crystal planes of [100], [002], [101], [102], [110], [103], [112], [201] and [004], respectively, for α–Mo_2C (no. 11–0680, PDF-2 Database).

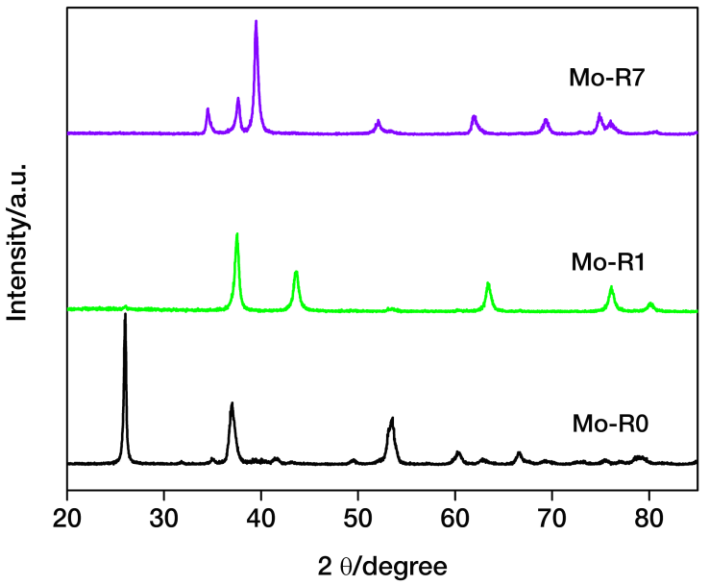

Figure S4. XRD patterns of the as–synthesized MoO_2 (Mo–R0), Mo_2N (Mo–R1), and Mo_2C (Mo–R7).

Table S2. Conditions and products, as well as sizes and morphologies of fifth-period transition metal carbides, nitrides, and oxides. Lattice, MP: Monoclinic Primitive; CP: Cubic Primitive; HP: Hexagonal Primitive.

Metal chloride	Urea/metal chloride molar ratio (R)	Product	Sinter temperature (°C) and time (h)	Morphology	Lattice	Diameter (nm) by XRD	Diameter (nm) by SEM
$ZrCl_4$	0	ZrO_2	800, 3		TP/MP		
	3	ZrO_2	800, 3		TP	16.9	
	9	ZrO_2	800, 3	particle	TP	19.9	10–200
	9	ZrO_2	1100, 3	particle	MP	41.1	20–100
$NbCl_5$	1	Nb_2O_5	800, 3	prism	OP	44.0	20–600
	5	NbN	800, 3	particle	CF	23.4	10–30
	12	NbC (N)	800, 3	particle	CF	12.0	10–20
$MoCl_5$	0	MoO_2	800, 3	particle	MP	28.0	10–40
	1	Mo_2N	800, 3	particle	CP	18.1	10–30
	5	Mo_2C	800, 3	vermiform	HP	19.5	15–100

Figure S5 gave the surface morphologies of the Mo, Nb, and Zr derivates. MoO_2 and Mo_2N particles interacted strongly and showed a tendency for aggregation. The Mo_2C had a worm–like appearance with an average size of 19.5 nm. Nb_2O_5 exhibited an anamorphic prism structure and these prisms adhered to each other chaotically. NbN particle was uniform, the particle size was 10–30 nm, and the particles locked to each other orderly. The particle size of NbC (N) was merely 10-20 nm and these particles

aggregated strongly. Tetragonal ZrO_2 was accumulated with nanoparticles showing strong aggregation. Compared to tetragonal ZrO_2, monoclinic ZrO_2 assumed a relative large particle size of 20–100 nm.

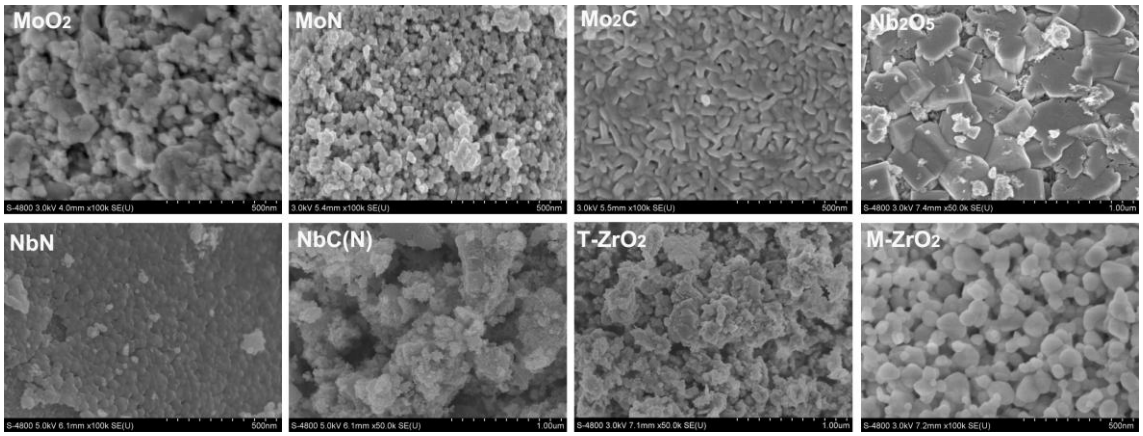

Figure S5. Surface morphologies of MoO_2, Mo_2N, Mo_2C, Nb_2O_5, NbN, NbC (N), tetragonal ZrO_2, and monoclinic ZrO_2.

The Effect of TiC Layer Thickness on the Performance of the DSCs

In our previous work, we found that the catalyst layer thickness affected the catalytic activities strongly. We prepared four kinds of TiC CEs on FTO glass with different TiC film thicknesses. Figure S6 showed that the four TiC film thicknesses were ca. 5, 10, 20, and 40 μm thick. We fabricated four DSCs with the four TiC CEs, named A (5μm), B (10 μm), C (20 μm), and D (40 μm). Figure S7 showed the *J-V* curves of these DSCs. The photovoltaic parameters for the four devices were Device A, V_{oc}=761 mV, J_{sc}=11.67 mA cm^{-2}, FF=0.38, PCE=3.37%; Device B, V_{oc}=781 mV, J_{sc}=12.19 mA cm^{-2}, FF=0.52, PCE=4.95%; Device C, V_{oc}=788 mV, J_{sc}=13.30 mA cm^{-2}, FF=0.62, PCE=6.50%; Device D, V_{oc}=762 mV, J_{sc}=13.87 mA cm^{-2}, FF=0.61, PCE=6.40%. It can be clearly seen that, the J_{sc} increased as the thickness increased, while V_{oc} changed a little in a scale of 761~788 mV. We found that the thickness impacted the FF and PCE significantly, which was in good agreement with previous work.[1] In a word, 20 μm TiC layer is enough for achieving a high catalytic activity and a subsequent highly performed DSC.

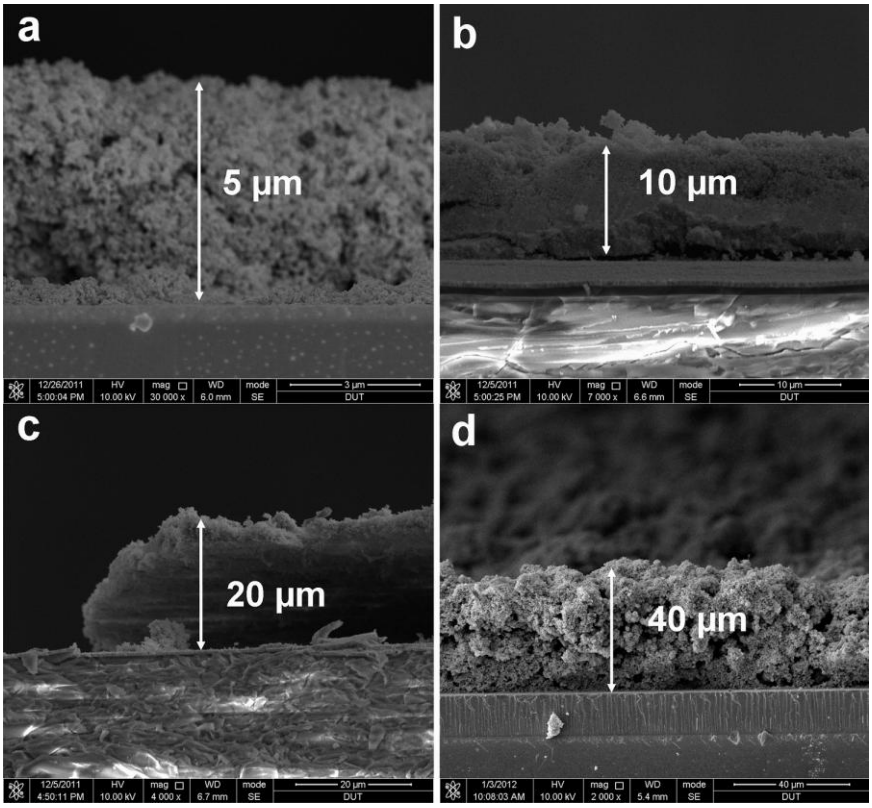

Figure S6. SEM image of the cross section of the counter electrodes with different TiC thicknesses. (a): 5 μm; (b): 10 μm; (c): 20 μm; (d): *4*0 μm. Bar in (a) is 3 μm, in (b) is 10 μm, in (c) is 20 μm, and in (d) is 40 μm.

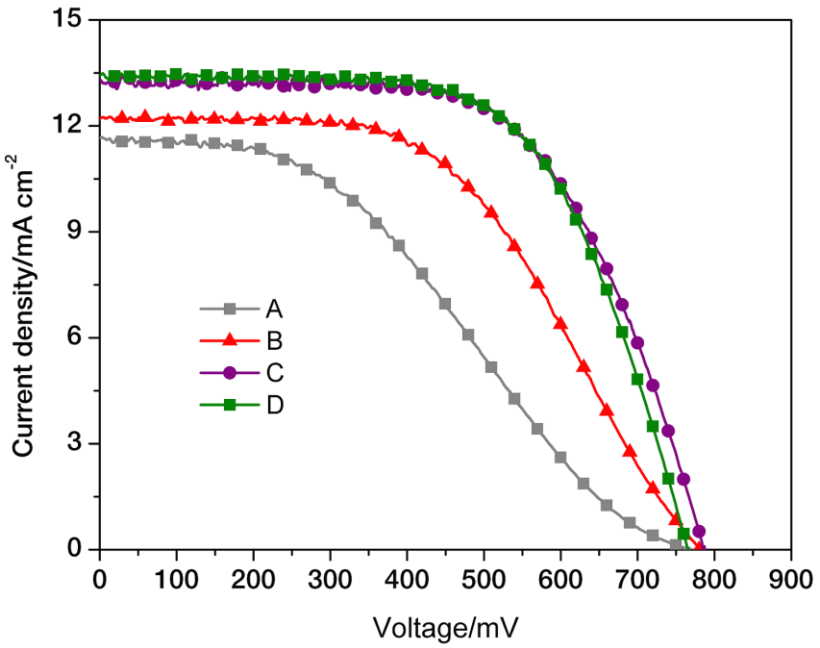

Figure S7. *J-V* curves of the I_3^-/I^- DSC based on TiC CE with different thicknesses (A): 5 μm, (B) 10 μm (C) 20 μm, and (D) 40 μm.

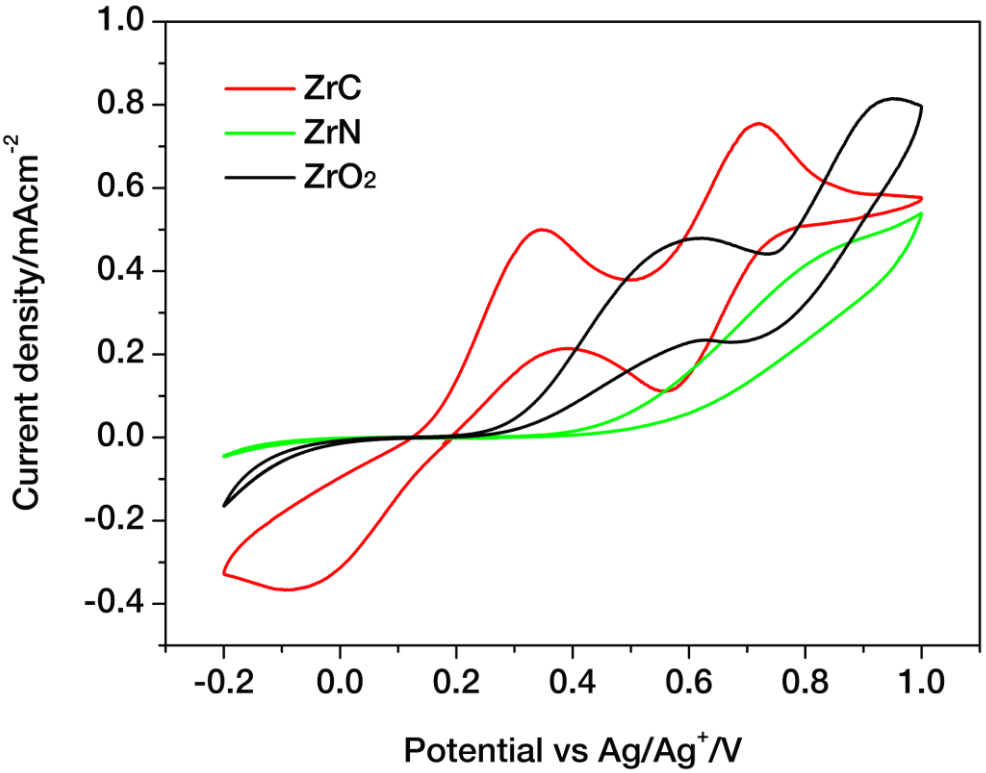

Figure S8. Cyclic voltammograms of the ZrC, ZrN, and ZrO_2 electrodes for I_3^-/I^- redox couple.

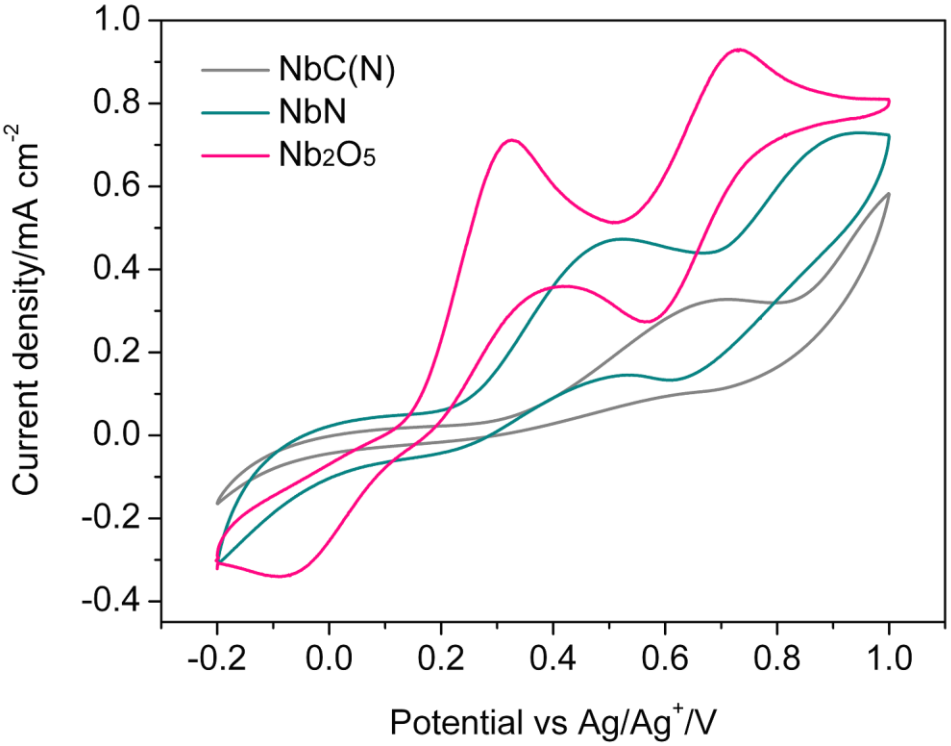

Figure S9. Cyclic voltammograms of the NbC (N), NbN, and Nb_2O_5 electrodes for I_3^-/I^- redox couple.

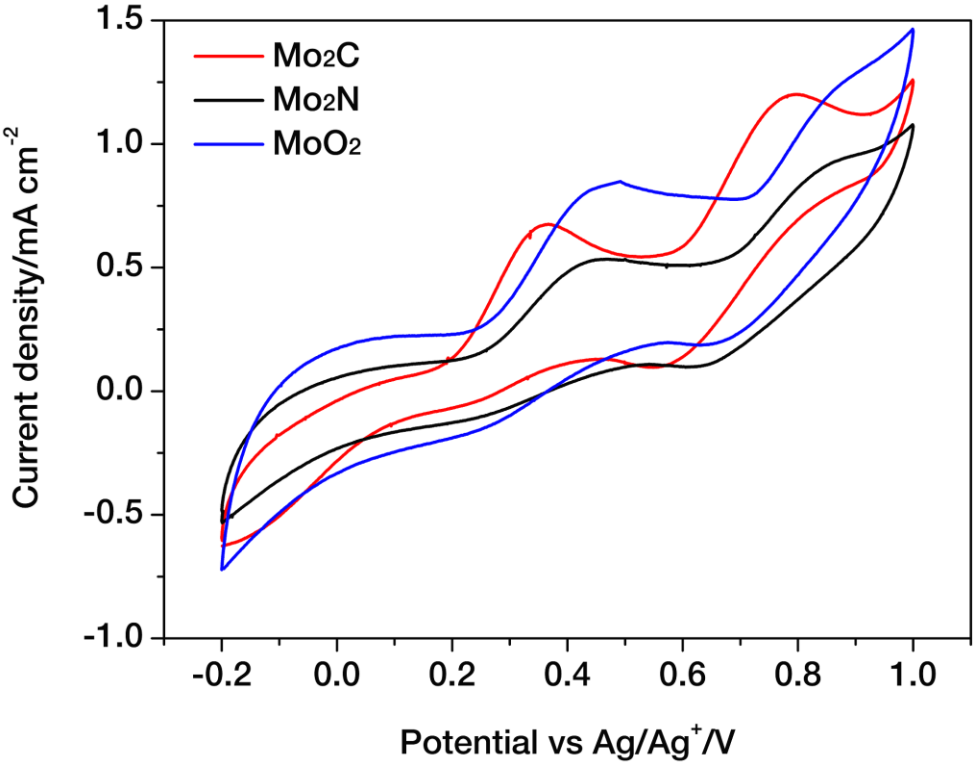

Figure S10. Cyclic voltammograms of the Mo_2C, Mo_2N, and MoO_2 electrodes for I_3^-/I^- redox couple.

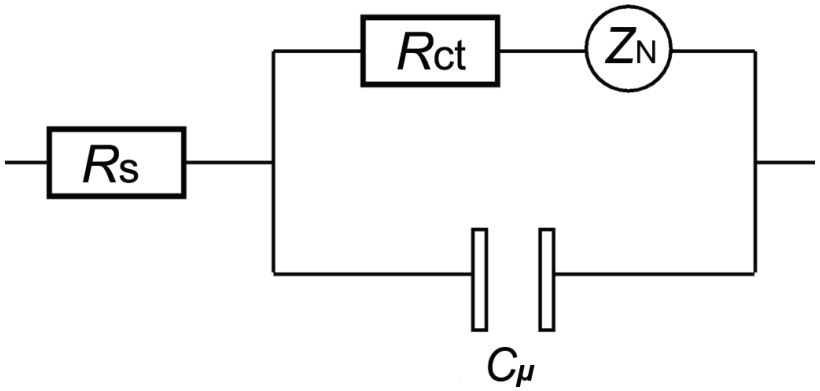

Figure S11. Equivalent circuit diagram used in EIS measurement.

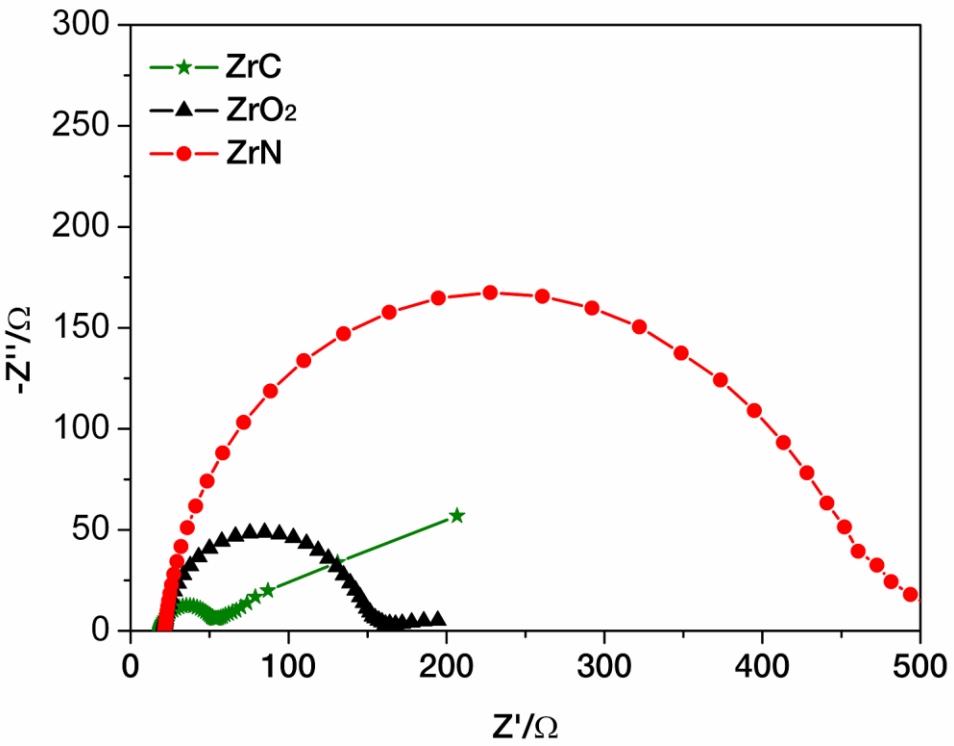

Figure S12. Nyquist plots of the I_3^-/I^- symmetrical cells based on two identical Zr derivate electrodes.

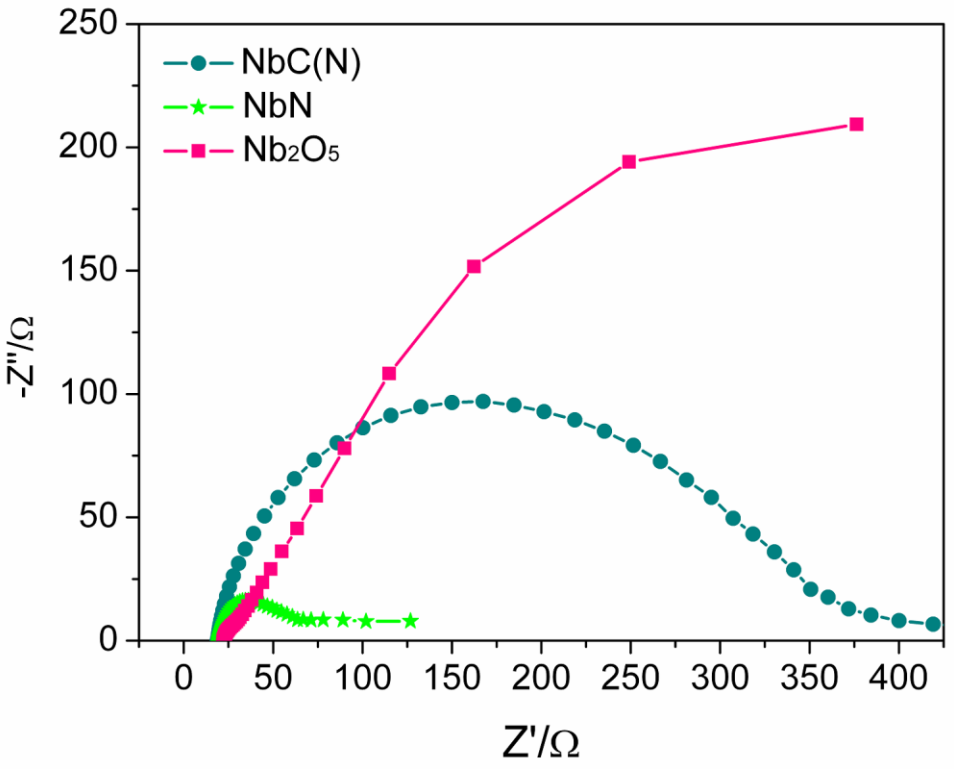

Figure S13. Nyquist plots of the I_3^-/I^- symmetrical cells based on two identical Nb derivate electrodes.

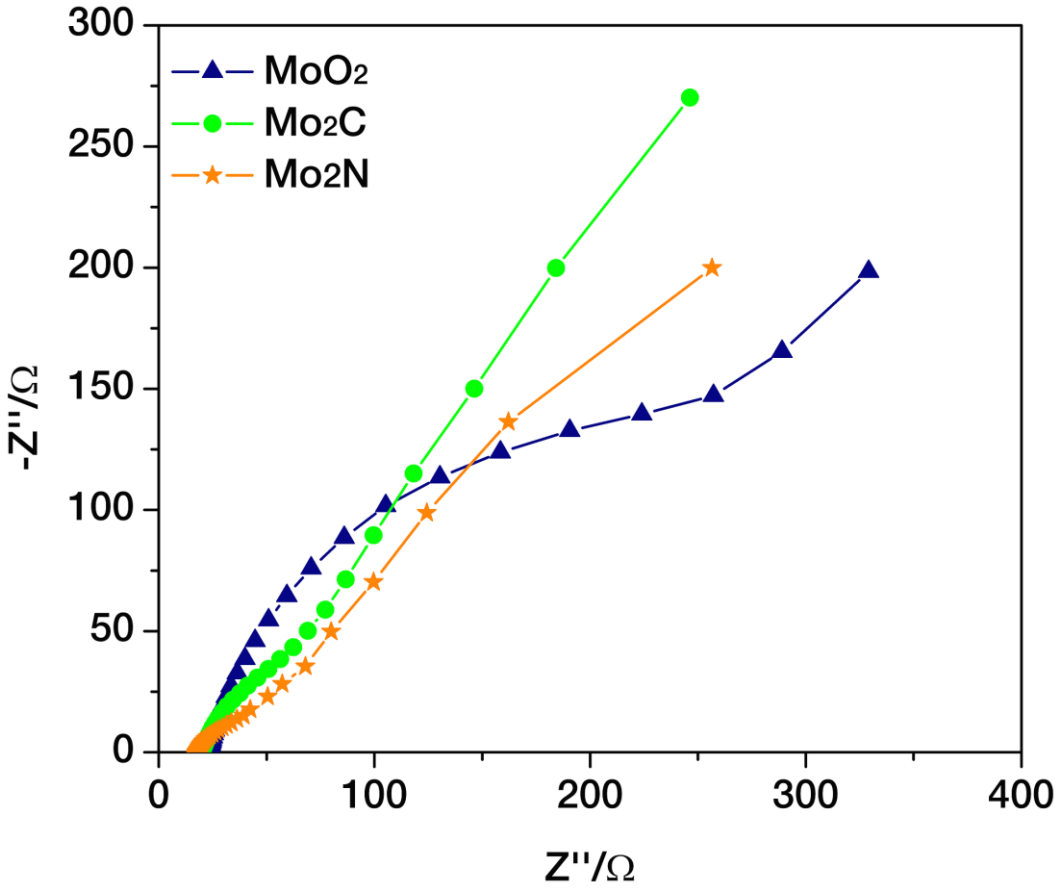

Figure S14. Nyquist plots of the I_3^-/I^- symmetrical cells based on two identical Mo derivate electrodes.

Table S3. EIS parameters of the I_3^-/I^- symmetrical cells based on two identical electrodes. [a] These materials are commercial.

CE catalysts	R_s/Ω	R_{ct}/Ω	$C_\mu/\mu F$	Z_N/Ω
TiC (N)	19.3	6.7	44.6	98.8
TiC[a]	20.7	5.1	66.5	110.0
TiN	22.5	11.2	68.5	84.7
TiO_2	33.5	693.2	37.2	810.1
VC (N)	18.3	6.2	77.5	12.4
VC[a]	21.2	20.8	10.5	350.3
VN	19.6	9.5	43.2	20.7
V_2O_3	19.3	10.4	53.7	69.7
VC–MC	20.5	2.9	298.0	9.4
Cr_2C_3	19.8	9.4	30.4	188.2
CrN	18.5	22.7	128.9	234.2
Cr_2O_3	27.9	503.9	21.1	726.0
ZrC[a]	18.5	36.6	48.9	149.7
ZrN	21.3	420.0	4.7	264.3
ZrO_2	20.6	121.1	8.7	172.3
NbC (N)	18.7	162.5	12.6	352.5
NbN	19.6	61.5	81.6	113.6
Nb_2O_5	21.9	20.9	47.7	302.0
MoO_2	22.5	74.5	28.2	405.2
Mo_2N	19.1	6.4	39.4	152.4
Mo_2C	17.3	8.1	29.7	184.5
Pt	21.13	4.7	12.3	6.8

Tafel Polarization Measurements

Tafel polarization curve can be divided into three zones. The curve at low potential (|U|<120 mV, in general) can be attributed to the polarization zone; the curve at middle potential (with a sharp slope) can be attributed to the Tafel zone; the curve at high potential (horizontal section) can be attributed to the diffusion zone. The latter two have a close relationship with the catalytic activities of the catalysts. In Figure S15, the intersection of the cathodic branch with the Y–axis can be considered as the limiting diffusion current density (J_{lim}). One can see that J_{lim} of Pt and TiC(N) is at the same order of magnitude. In addition, in the Tafel zone, the intersection of the cathodic branch and the equilibrium potential line (black solid line) can be considered as the exchange current density (J_0). As shown in Figure S15, the J_0 of Pt is larger than that of TiC(N). This means Pt is more effective than TiC(N) in catalyzing the I_3^- reduction.

In theory, J_0 varies inversely with R_{ct} as shown in eq (S1). The variation of J_0 obtained from Tafel polarization measurements is generally in accordance with the change tendency of R_{ct} obtained from EIS measurements. On the basis of eq (S2, S3), J_{lim} has a positive relation with the diffusion coefficient (D, illustrating the diffusion character of the redox couple in the electrolyte), which is correlated negatively with the diffusion impedance (Z_N). The EIS and Tafel polarization results demonstrate that the J_{lim} variation of different materials is generally agreement with the change tendency of Z_N.

$$J_0 = \frac{RT}{nFR_{ct}} \qquad \text{(S1)}$$

where R is the gas constant, T is the temperature, F is Faraday's constant, n is the electron number involving in the reaction, and R_{ct} is the charge transfer resistance.

$$D = \frac{l}{2nFC} J_{lim} \qquad \text{(S2)}$$

where D is the diffusion coefficient of the triiodide, l is the spacer thickness, C is the triiodide concentration, and n, F retain their established meanings.

$$Z_N = \frac{W}{\sqrt{i\omega}} \tanh\left(\sqrt{\frac{i\omega}{K_N}}\right) \quad \text{(S3)}$$

where $W = kT / n^2 e^2 CA\sqrt{D}$; $K_N = D / \delta^2$, k is the Boltzmann constant, e is the elementary charge, and δ is the thickness of the diffusion layer. D, C, n retain their established meanings

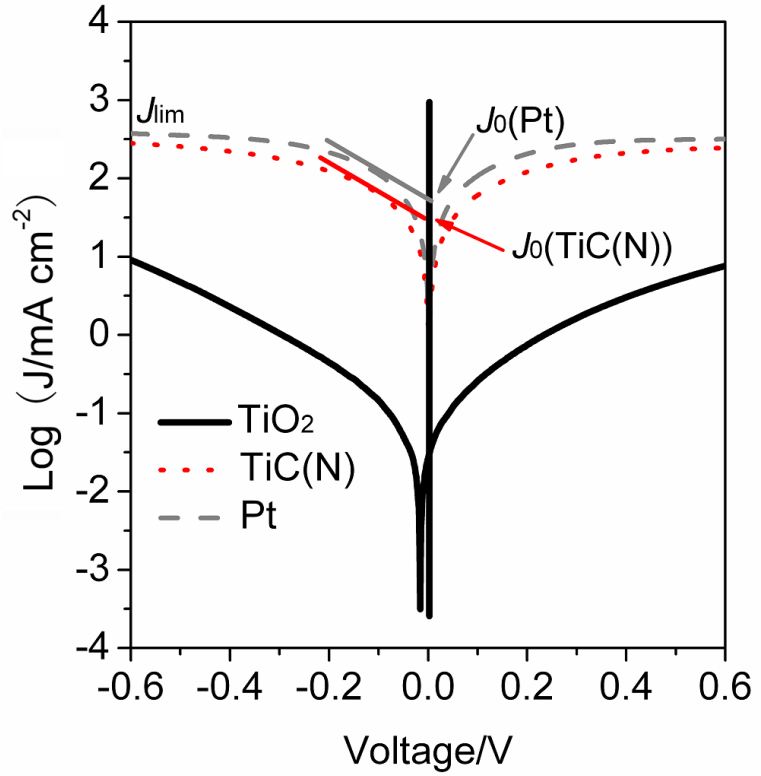

Figure S15. Tafel polarization curves of the I_3^-/I^- symmetrical cells fabricated with two identical Pt electrodes, TiO_2, orl TiC (N) electrodes.

Table S4. Photovoltaic parameters of the T_2/T^- DSCs using various carbides counter electrodes and The EIS parameters of the T_2/T^- symmetrical cells.

CE	V_{oc}/mV	J_{sc}/mA cm^{-2}	FF	PCE/%	R_s/Ω	R_{ct}/Ω	C_μ/μF	Z_N/Ω
Pt	625	12.23	0.48	3.66	15.0	35.1	21.8	45.2
TiC	629	12.44	0.63	4.96	22.7	5.1	78.5	24.9
VC-MC	633	12.86	0.63	5.15	23.2	4.8	181.1	36.6
VC	647	11.79	0.54	4.06	23.3	24.9	44.5	26.0
Cr_3C_2	641	10.84	0.65	4.54	23.2	14.0	65.4	73.5

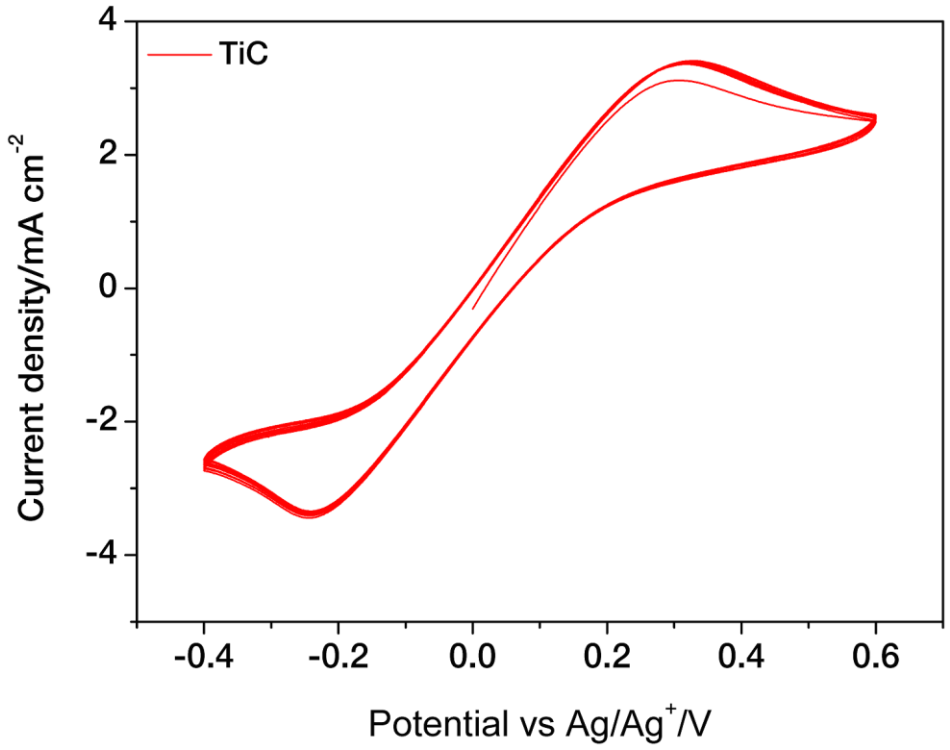

Figure S16. 10 Consecutive cyclic voltammograms of the TiC electrode for T_2/T^- spices.

Reference

(1) Murakami T. N.; Grätzel M. *Inorg. Chim. Acta* **2008**, *361*, 572-580.